A mass–conserving algorithm for dynamical lubrication problems with cavitation

Roberto F. Ausas[a], Mohammed Jai[b] and Gustavo C. Buscaglia[c]

[a]Centro Atómico Bariloche and Instituto Balseiro,
8400, Bariloche, Argentina
e-mail: rfausas@gmail.com,

[b]CNRS-UMR 5208, Mathématiques, INSA de LYON
Bat Leonard de Vinci, F-69621 Villeurbanne, France
e-mail: mohammed.jai@insa-lyon.fr

[c]ICMC, Universidade de São Paulo
13560-970 São Carlos, SP, Brazil
e-mail: gustavo.buscaglia@icmc.usp.br

December 12, 2008

Abstract

A numerical algorithm for fully–dynamical lubrication problems based on the Elrod–Adams formulation of Reynolds equation with mass–conserving boundary conditions is described. A simple but effective relaxation scheme is used to update the solution maintaining the complementarity conditions on the variables that represents the pressure and fluid fraction. The equations of motion are discretized in time using Newmark's scheme, and the dynamical variables are updated within the same relaxation process just mentioned. The good behavior of the proposed algorithm is illustrated in two examples: Oscillatory squeeze flow (for which the exact solution is available) and a dynamically loaded journal bearing. This article is accompanied by the ready–to–compile source code with the implementation of the proposed algorithm, which is publicly available at `www.lcad.icmc.usp.br/~buscaglia/download`.

Nomenclature

Notice that all quantities are non–dimensional.

B Bush width.

x_1	Longitudinal coordinate (along the sliding direction).
x_2	Transverse coordinate.
h	Gap thickness function.
$H(t)$	Uniform gap thickness at time t in the oscillatory–squeeze flow example.
M	Journal mass.
p	Pressure field.
p_a	Feeding pressure.
$p_{i,j}^{n,k}$	Discrete pressure at node i,j at iteration k of time step n.
θ	Fluid fraction field.
$\theta_{i,j}^{n,k}$	Discrete fluid fraction at node i,j at iteration k of time step n.
$\mathbf{p}^{n,k}$, $\theta^{n,k}$	Vectors of nodal values of p and θ at iteration k of time step n.
N_1, N_2	Number of grid cells along x_1 and x_2 directions.
Δx_1, Δx_2	Grid spacing along x_1 and x_2 directions.
Δt	Time step.
X, Y	Position of the journal center at time t.
$X^{n,k}$, $Y^{n,k}$	Discrete position of the journal center at iteration k of time step n.
$\overline{W}$	Load carrying capacity $[N]$.
W_X^a, W_Y^a	X and Y components of the applied load.
W_X, W_Y	X and Y components of the load carrying capacity.
ω_p, ω_θ	Relaxation parameters for pressure and fluid fraction.
Ω	Non-dimensional computational domain.
Ω^+	Active region.
Ω_0	Cavitated region.
Γ_0	Outlet boundary.
Γ_a	Feeding boundary.

1 Introduction

Significant progress has been made over the last decades in the field of numerical modeling of lubricated devices. The mass–conserving Elrod–Adams model [1] is by now well–established as the accurate tool for simulation in hydrodynamic lubrication involving cavitation. This model contains two unknown fields, one of which is the pressure p and the other the fluid fraction variable that will be denoted by θ, which takes values between zero and one. These variables satisfy complementarity–like conditions: In the pressurized region Ω^+ of the bearing ($p > 0$) the film is complete ($\theta = 1$), whereas in the cavitated region (incomplete film, i.e., $\theta < 1$), denoted by Ω_0, the pressure is zero ($p = 0$). At the internal boundary Σ between these two regions (cavitation boundary), which is an unknown of the problem, the mathematical conditions are the continuity of the pressure (p tends to zero when approaching Σ from either side) and the conservation of the mass of lubricant. Notice that Ω^+, Ω_0, and thus Σ, change with time. It should be kept in mind that several complex phenomena, involving a wide range of spatial and temporal scales, take place

in the cavitated region. The above complementarity conditions are of course only approximations to the true physics. Recent attempts at incorporating a more sophisticated description of bubble nucleation may lead to improvement (see e.g. Geike and Popov [2]).

The Elrod–Adams p–θ model can also be simply regarded as a set of mass–conserving boundary conditions for Reynolds lubrication equation. These are usually called the *JFO boundary conditions* honoring the pioneer work of Jacobson and Floberg[3] and Olsson[4]. The fluid fraction field θ in the model can be seen as an auxiliary quantity that is used to determine the correct conditions to be applied on Σ. Another possibility is given, instead, by the imposition of the so–called *Reynolds boundary conditions* at Σ (both the pressure and its normal derivative required to vanish at Σ), which are much easier to deal with numerically at the expense of not enforcing the conservation of the mass of lubricant. In many cases the two models yield very similar results. Ausas *et al* [5], however, have recently shown that for the increasingly popular micro–textured bearings the use of a mass–conserving model is mandatory. Later on, an example showing that mass–conservation is also crucial in untextured bearings if transient effects are strong is provided.

The main difficulty concerning the mass–conserving model comes from its highly nonlinear nature. The nonlinearity of the mathematical problem, combined with the discretization errors inherent to the numerical approximation (be it finite differences, finite volumes, finite elements, etc.) leads to nonlinear algebraic problems for which lack of convergence of iterative methods is frequent. The interaction of the discretization scheme with the nonlinear iteration strategy makes the behavior of the simulation codes quite dependent on the implementation details, which cannot be fully described in journal articles. Though many algorithms have been published in the literature (see, among others, [6, 7, 8, 9, 10]), the codes implementing them are not publicly available. Public availability of source codes is an important step towards the maturity of numerical techniques in any area of engineering simulation. In this paper, the numerical solution of the mass–conserving lubrication model with the $p - \theta$ formulation of Elrod and Adams [1] for dynamically–loaded bearings is addressed. A relaxation–type finite–volume–based algorithm that has proven to be accurate and robust in several industrial applications is described. Further, the source code is made freely available from the Web, in such a way that any interested reader can download it, study the implementation details, reproduce the nontrivial examples that are discussed in the next sections, and even modify the code to run more sophisticated examples or test algorithmic variants.

The plan of the article is as follows: In Section 2, the mathematical model in the case of an arbitrary, time–dependent gap–thickness $h(x_1, x_2, t)$ is briefly recalled. In Section 3 the numerical algorithm is described under the simplifying assumption of $h(x_1, x_2, t)$ being known *a priori*. This is illustrated in Section 4, in which the code is applied to an example for which the exact solution is computable (oscillatory squeeze flow), also including the results of the non–mass–conserving model (Reynolds boundary conditions) for comparison. The proposed methodology is then extended to the fully dynamical case of a journal bearing under time–dependent load, as detailed in Section 5, followed by an application example in Section 6.

2 Mathematical model and numerical treatment

2.1 Governing equations

The problem to be considered is that of a hydrodynamic bearing with a time–dependent gap thickness $h(x_1, x_2, t)$. The x_1-axis is chosen parallel to the (fixed) sliding velocity, and the proximity domain Ω is assumed to be a rectangle in the (x_1, x_2) coordinates. Throughout this article all variables are non–dimensional. The well–known mass–conserving mathematical model (in the $p - \theta$ form proposed by Elrod & Adams [1]) reads

$$div\ \left(h^3 \nabla p\right) = \alpha \frac{\partial(\theta\, h)}{\partial x_1} + 2\ \frac{\partial(\theta h)}{\partial t} \qquad in\ \Omega \setminus \Sigma \tag{1}$$

$$p \geq 0, \qquad \theta = 1 \qquad in\ \Omega^+ \tag{2}$$

$$p = 0, \qquad \theta < 1 \qquad in\ \Omega_0 \tag{3}$$

$$p = 0 \qquad on\ \Sigma \tag{4}$$

$$p = p_a \qquad on\ \ \Gamma_a \ \ \text{(feeding)} \tag{5}$$

$$p = 0 \qquad on\ \ \Gamma_0 \ \ \text{(oil outlet)} \tag{6}$$

supplemented with the mass–conservation condition at the cavitation boundary

$$(h_0\, \theta_0 - h_+)\ \ \alpha\, \hat{e}_1 \cdot \hat{n} + h_+^3 \left(\frac{\partial p}{\partial n}\right)_+ = 2\, (h_0\, \theta_0 - h_+)\ \ V_n \qquad on\ \ \Sigma \tag{7}$$

where α is the non–dimensional sliding velocity, assumed parallel to $\hat{e}_1$, the unit vector parallel to x_1, $\hat{n}$ is the unit vector normal to Σ, oriented outwards from Ω^+, V_n represents the local normal velocity at which Σ is moving, and the subscripts 0 and + refer to the limit values of the variables as Σ is approached from the cavitated and active regions, respectively. The above set of equations and boundary conditions is solved in time starting from an initial condition

$$\theta(x_1, x_2, t = 0) = \theta_0(x_1, x_2) \tag{8}$$

at all points belonging to $\Omega_0(t = 0)$, the initial cavitated region. The mathematical analysis of this model has been rigorously carried out by Bayada and Chambat[11, 12].

2.2 Discrete formulation

The computational domain is assumed to be the rectangle

$$\Omega = (0, 1) \times (0, B) \tag{9}$$

on which a uniform, cartesian mesh of $N_1 \times N_2$ nodes, with spacing $\Delta x_1 = 1/N_1$ and $\Delta x_2 = B/N_2$ is defined. Subscripts i and j at a variable refer to its value at the discrete location $(x_1)_i = i\, \Delta x_1$, $(x_2)_j = j\, \Delta x_2$.

The x_1 component of the flux going from node $(i - 1, j)$ to node (i, j) is approximated by

$$-h^3 \frac{\partial p}{\partial x_1} + \alpha\, h\, \theta \ \simeq\ -\frac{h_{i-1,j}^3 + h_{i,j}^3}{2}\ \ \frac{p_{i,j} - p_{i-1,j}}{\Delta x_1} + \alpha\, h_{i-1,j}\, \theta_{i-1,j} \tag{10}$$

Notice that in the second term both h and θ are taken at node $(i-1,j)$, which provides upwinding since the sliding velocity is assumed from left to right. A generalization of the algorithm that allows for a sliding velocity from right to left is straightforward and has been omitted for the sake of brevity. The approximation of the x_2 component of the flux going from node (i,j) to node $(i,j+1)$ reads

$$-h^3\frac{\partial p}{\partial x_2} \quad \simeq \quad -\frac{h^3_{i,j+1}+h^3_{i,j}}{2}\ \frac{p_{i,j+1}-p_{i,j}}{\Delta x_2} \tag{11}$$

The time variable is discretized into uniform time steps of length Δt, and a superscript n on a variable refers to its value at time $t_n = n\Delta t$. Combining the spatial and temporal discretizations above in an implicit scheme, the following discrete equation for mass conservation at node (i,j) can be obtained:

$$\begin{aligned} 2\ \Delta x_1^2\ \frac{c^n_{i,j}-c^{n-1}_{i,j}}{\Delta t}+\alpha\ \Delta x_1\ (c^n_{i,j}-c^n_{i-1,j}) \ &= \ s^n_{i,j}\ p^n_{i+1,j}-\left(s^n_{i,j}+s^n_{i-1,j}\right)\ p^n_{i,j}+s^n_{i-1,j}\ p^n_{i-1,j}\ + \\ &+\ q^2\ \left[s^n_{i,j+1}\ p^n_{i,j+1}-(s^n_{i,j+1}+s^n_{i,j})\ p^n_{i,j}+s^n_{i,j}\ p^n_{i,j-1}\right] \end{aligned} \tag{12}$$

where

$$s_{i,j}=\frac{h^3_{i,j}+h^3_{i+1,j}}{2}, \qquad c_{i,j}=\theta_{i,j}\ h_{i,j}, \qquad q=\frac{\Delta x_1}{\Delta x_2} \tag{13}$$

Notice that, since the scheme is based on the mass balance at each node with uniquely–defined fluxes, it is automatically mass–conserving. The complementarity conditions for the discrete variables are, for all i, j and n:

$$0\le p^n_{i,j}, \qquad 0\le\theta^n_{i,j}\le 1, \tag{14}$$

$$p^n_{i,j}>0 \ \ \Rightarrow \ \ \theta^n_{i,j}=1, \tag{15}$$

or, equivalently,

$$\theta^n_{i,j}<1 \ \ \Rightarrow \ \ p^n_{i,j}=0 \tag{16}$$

From this it is clear that cavitation will always take place at the grid nodes.

Considering $h(x_1,x_2,t)$ known, and $p^{n-1}_{i,j}$, $\theta^{n-1}_{i,j}$ already available at all nodes from the previous time step, it is not obvious at all that new nodal values $p^n_{i,j}$, $\theta^n_{i,j}$ exist satisfying the equation (12) and the boundary conditions, together with the complementarity conditions (14)-(15), but an existence analysis is out of the scope of this article. It is assumed that a discrete solution does exist, and discussed next an iterative algorithm to determine it.

2.3 Iterative algorithm

The proposed algorithm is adapted from the one used in [5] for the steady case. The nodal variables are obtained as limits of an iterative process, so that adding a second superscript to denote the iteration number the algorithm reads:

Find $p^n_{i,j}$, $\theta^n_{i,j}$, for $i=1,2,...,N_1$, and $j=1,2,\ldots,N_2$ as

$$(p^n_{i,j},\theta^n_{i,j})=\lim_{k\to\infty}(p^{n,k}_{i,j},\theta^{n,k}_{i,j}), \qquad (p^{n,0}_{i,j},\theta^{n,0}_{i,j})=(p^{n-1}_{i,j},\theta^{n-1}_{i,j})$$

To describe the way in which the k-th iterate is built let us first define $P_{i,j}^{n,k}$ and $\Theta_{i,j}^{n,k}$, which are intermediate values of the pressure p and of the fluid fraction field θ that are obtained from Eq. (12) by elimination of the nodal values with all other unknowns frozen at the previous iteration. They are thus given by

$$\begin{aligned} P_{i,j}^{n,k} &= \frac{1}{s_{i,j}^{n,k-1}+s_{i-1,j}^{n,k-1}+q^2(s_{i,j+1}^{n,k-1}+s_{i,j}^{n,k-1})}\Big\{-2\,\Delta x_1^2\,\frac{c_{i,j}^{n,k-1}-c_{i,j}^{n-1}}{\Delta t}-\alpha\,\Delta x_1\,(c_{i,j}^{n,k-1}-c_{i-1,j}^{n,k-1})+ \\ &\quad +s_{i,j}^{n,k-1}\,p_{i+1,j}^{n,k-1}+s_{i-1,j}^{n,k-1}\,p_{i-1,j}^{n,k-1}+q^2\,\left(s_{i,j+1}^{n,k-1}\,p_{i,j+1}^{n,k-1}+s_{i,j}^{n,k-1}\,p_{i,j-1}^{n,k-1}\right)\Big\} \end{aligned} \tag{17}$$

$$\begin{aligned} \Theta_{i,j}^{n,k} &= \frac{1}{\left(\frac{2\Delta x_1^2}{\Delta t}+\alpha\,\Delta x_1\right)h_{ij}^n}\left\{\frac{2\Delta x_1^2 c_{ij}^{n-1}}{\Delta t}+\alpha\,\Delta x_1\,c_{i-1,j}^{n,k-1}+\right. \\ &\quad +s_{i,j}^n\,p_{i+1,j}^n-\left(s_{i,j}^n+s_{i-1,j}^n\right)p_{i,j}^n+s_{i-1,j}^n\,p_{i-1,j}^n\;+ \\ &\quad \left.+q^2\,\left[s_{i,j+1}^n\,p_{i,j+1}^n-(s_{i,j+1}^n+s_{i,j}^n)\,p_{i,j}^n+s_{i,j}^n\,p_{i,j-1}^n\right]\right\} \end{aligned} \tag{18}$$

The proposed algorithm consists of a relaxation scheme combined with corrections to enforce the complementarity conditions (14)-(15). Please find the algorithm detailed in pseudo–code form in Table 1. In the authors' experience, the relaxation parameters ω_p and ω_θ do not need fine tuning. All applications that have been run up to now converged well with the choice $\omega_p = \omega_\theta = 1$. If necessary, a relaxation parameter different than 1 can easily be specified in the computational codes provided.

3 First example: Oscillatory squeeze flow

The one–dimensional system shown in Fig. 1 is considered, consisting of two parallel plates in the region $\Omega = [0, 1]$. This is a well–known benchmark which has previously been considered by other authors[13, 9]. The plate at the bottom is at rest, while the one at the top is moving vertically ($\alpha = 0$) with a prescribed function of time, i.e.

$$h(x_1, x_2, t) = H(t) = 0.125\;cos(4\,\pi\,t) + 0.375 \tag{19}$$

The following boundary conditions are imposed

$$p(x_1 = 0, x_2, t) = p(x_1 = 1, x_2, t) = p_0 = 0.025 \tag{20}$$

and periodic conditions in $x_2 = 0$ and $x_2 = B$ (to solve the 1D problem with the 2D code). The initial condition (at $t = 0$) is that of full film ($\theta = 1$ everywhere).

Table 1: Iterative algorithm.

do $(n = 1, \ldots, NT)$ *(Loop over time steps)*
  $t_n \;=\; n\,\Delta t, \quad k \;=\; 0$
  do $(i = 1, \ldots, N_1,\ j = 1, \ldots, N_2)$
    $h_{ij}^{n} \;=\; h(i\Delta x_1, j\Delta x_2, t_n), \quad p_{ij}^{n,0} \;=\; p_{ij}^{n-1}, \quad \theta_{ij}^{n,0} \;=\; \theta_{ij}^{n-1}$
  end do
  do while (*change* $>$ *tolerance*) *(Relaxation)*
    $k \;\leftarrow\; k+1$
    do $(i = 1, \ldots, N_1,\ j = 1, \ldots, N_2)$
      if $(p_{i,j}^{n,k-1} > 0$ *or* $\theta_{i,j}^{n,k-1} == 1)$ ***then***
        Compute $P_{i,j}^{n,k}$ *using Eq. (17)*
        $p_{i,j}^{n,k} \;=\; \omega_p\, P_{i,j}^{n,k} + (1-\omega_p)\, p_{i,j}^{n,k-1}$
        if $(p_{i,j}^{n,k} \geq 0)$ *(cavitation check)*
          $\theta_{i,j}^{n,k} = 1$
        else
          $p_{i,j}^{n,k} = 0$
        end if
      end if
      if $(p_{i,j}^{n,k} \leq 0$ *or* $\theta_{i,j}^{n,k} < 1)$ ***then***
        Compute $\Theta_{i,j}^{n,k}$ *using Eq. (18)*
        $\theta_{i,j}^{n,k} \;=\; \omega_\theta\, \Theta_{i,j}^{n,k} + (1-\omega_\theta)\, \theta_{i,j}^{n,k-1}$
        if $(\theta_{i,j}^{n,k} < 1)$ *(cavitation check)*
          $p_{i,j}^{n,k} = 0$
        else
          $\theta_{i,j}^{n,k} = 1$
        end if
      end if
    end do
    change $\;=\; ||\mathbf{p}^{n,k} - \mathbf{p}^{n,k-1}||_2 + ||\theta^{n,k} - \theta^{n,k-1}||_2$
  end do
  do $(i = 1, \ldots, N_1,\ j = 1, \ldots, N_2)$
    $p_{ij}^{n} \;=\; p_{ij}^{n,k}, \quad \theta_{ij}^{n} \;=\; \theta_{ij}^{n,k}$
  end do
end do *(End Loop over time steps)*

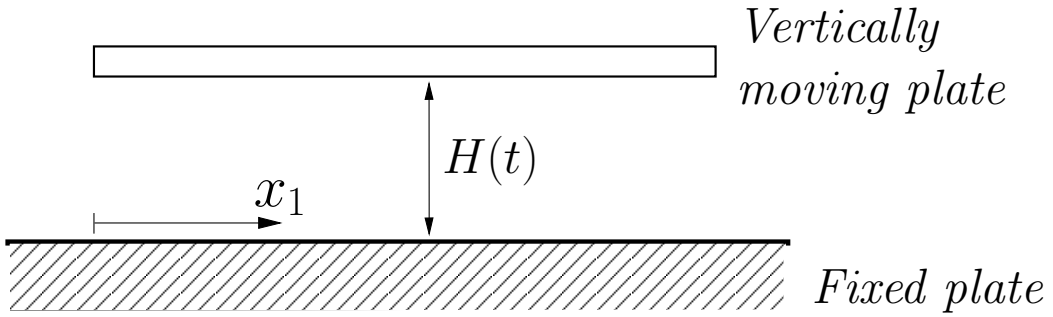

Figure 1: One dimensional system considered for the squeeze–flow example.

The exact solution to this problem exhibits a cavitated region that nucleates shortly after $t = 0.25$ (in fact, at $t_{rup} = 0.250079$) at $x = 0.5$. Let us denote by $\Sigma(t)$ the position at time t of the right boundary of Ω_0. Since the problem is symmetric with respect to $x = 0.5$, the left boundary is located at $1 - \Sigma(t)$. The cavitated region grows from t_{rup} to $t_{ref} = 0.314826$ according to

$$\Sigma(t) = 1 - \left[\frac{p_0\ H^3(t)}{H'(t)}\right]^{1/2} \tag{21}$$

This can easily be obtained from the condition $\partial p/\partial n = 0$ at $\Sigma(t)$, which in this case holds for the rupture boundary. After t_{ref} reformation starts and the cavitation boundary receeds until the cavitated region disappears shortly before $t = 0.75$. This process repeats periodically, with period $T = 0.5$. The exact solution for the reformation stage is more difficult to obtain than the corresponding one for the rupture process. In this case, by using Eq. (7) one arrives at a differential equation of the form $\Sigma'(t) = \mathcal{F}\left(p_0, H(t), \theta(\Sigma(t), t), \Sigma(t)\right)$. To solve this equation one stores the time at which film rupture happened for each position, since it is needed to compute $\theta(\Sigma(t), t)$. Besides this, integration is straightforward (the approach used in [9] can also be adopted). A comparison of the exact solution with numerical results obtained with the proposed algorithm is shown in Fig. 2. Part (a) of this figure shows the film thickness (Eq. (19)) after $t = 0.25$. In part (b), a plot of the exact $\Sigma(t)$ predicted by the model is shown, superimposed to that obtained numerically with $\Delta x_1 = 1/450$ and $\Delta t = 6.6 \times 10^{-4}$. It can be seen that the numerical results closely follow the exact solution, although with a staircase pattern since by construction the numerical cavitation boundary is located at a mesh node.

To illustrate the crucial role of mass–conservation in this problem, part (c) of Fig. 2 shows similar plots corresponding to the non–mass–conserving Reynolds model (i.e., boundary conditions $p = \partial p/\partial n = 0$ at $\Sigma(t)$). It is obvious that Reynolds model largely overestimates the speed at which the film reforms. Regarding the computational cost for this case, the algorithm takes 5 minutes on a Pentium IV (3.0 GHz) processor to complete one cicle of the oscillatory movement. This cost is dominated by the slow convergence of the Gauss-Seidel iterations when the active region is large, and could be reduced by cleverly switching to some other iterative scheme in that region.

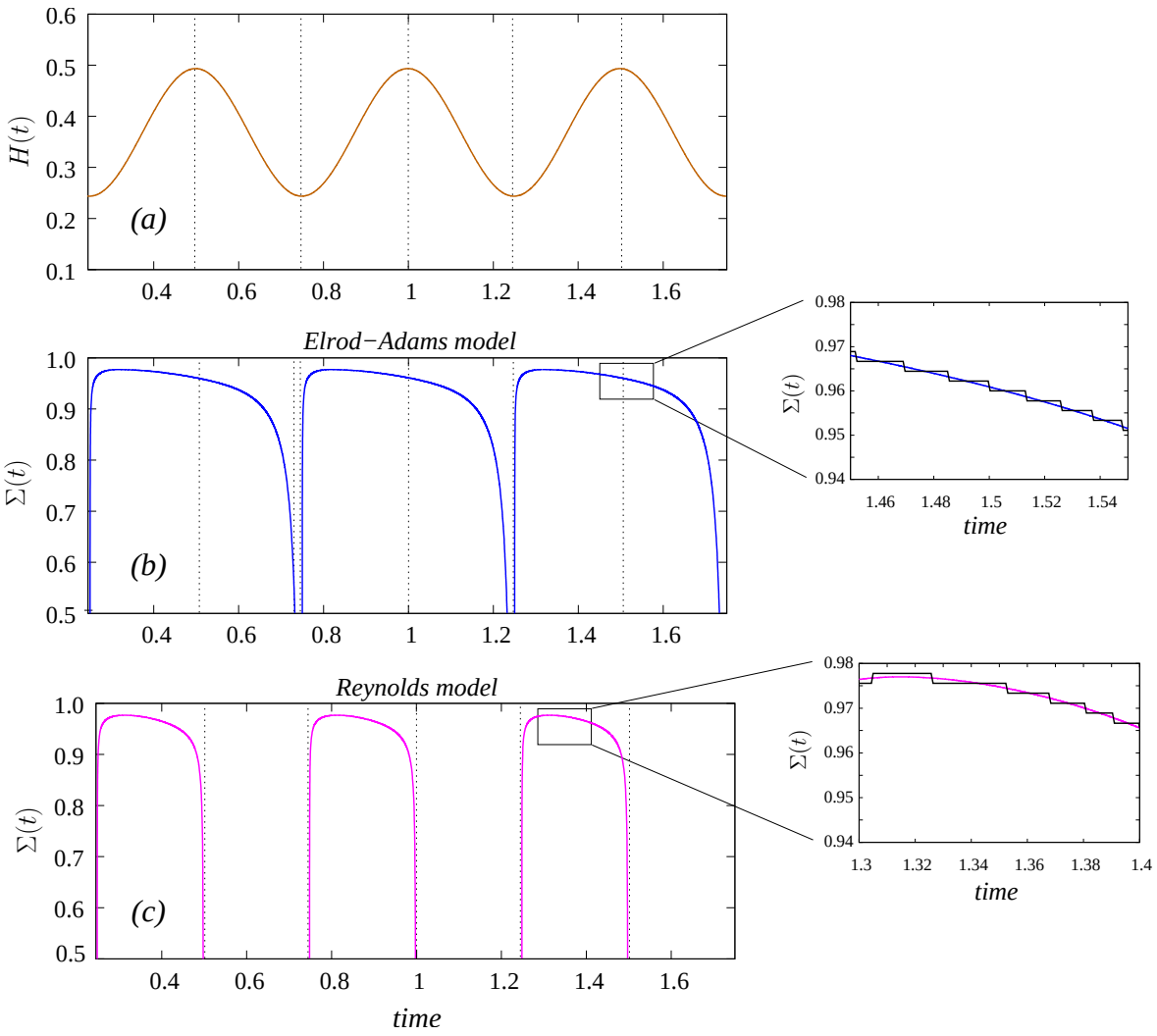

Figure 2: (a) Film thickness $H(t)$ used in the oscillatory squeeze flow example. (b) Right cavitation boundary $\Sigma(t)$ for the mass–conserving Elrod–Adams model, comparing the numerical result to the exact solution. (c) Same as part (b) for non–mass–conserving Reynolds model. Notice the detail in (b) and (c), showing the staircased shape of the numerical cavitation boundary.

4 Extension to dynamical problems

4.1 The journal bearing

Now, let consider the case in which the relative position of the bearing surfaces, and thus also the film–thickness function $h(x_1, x_2, t)$, results from the dynamical interaction of the bearing with an applied load.

To demonstrate such a problem, a journal bearing centered at the origin is considered. $(X(t), Y(t))$ denote the position of the shaft's center at time t. With the geometry of the problem as defined in Fig. 3, the film–thickness function over the domain (which is the rectangle $\Omega = (0, 1) \times (0, B)$)

is given by

$$h(x_1, x_2, t) = 1 + X(t)\cos(2\pi x_1) + Y(t)\sin(2\pi x_1) \tag{22}$$

and the boundary conditions

$$p(x_1, x_2 = B, t) = p_a \tag{23}$$
$$p(x_1, x_2 = 0, t) = 0 \tag{24}$$

with periodicity imposed on $x_1 = 0$ and $x_1 = 1$.

Denoting by $W_X^a(t)$ and $W_Y^a(t)$, respectively, the X and Y components of the applied load, and by M the mass of the shaft, the dynamical equations for $X(t)$ and $Y(t)$ read

$$M\,\frac{d^2X}{dt^2} = W_X(t) + W_X^a(t) \tag{25}$$
$$M\,\frac{d^2Y}{dt^2} = W_Y(t) + W_Y^a(t) \tag{26}$$

where $W_X(t)$ and $W_Y(t)$ are given by

$$W_X(t) = \int_\Omega p(x_1, x_2, t)\ \cos(2\pi x_1)\ d\Omega \tag{27}$$
$$W_Y(t) = \int_\Omega p(x_1, x_2, t)\ \sin(2\pi x_1)\ d\Omega \tag{28}$$

Notice the strong coupling between (25)-(26) and the lubrication problem (1)-(7) through the pressure field $p(x_1, x_2, t)$.

4.2 Algorithm

The algorithm detailed in Table 1 needs to be modified for the fully dynamical case, since the film–thickness function $h(x_1, x_2, t)$ is now an unknown of the problem, computed from $X(t)$ and $Y(t)$ using (22).

The adopted method is based on the following Newmark-scheme for (25)-(26):

$$X^n = X^{n-1} + \Delta t\, U^{n-1} + \frac{\Delta t^2}{2\ M}\ (W_X^n + W_X^a(t_n)) \tag{29}$$
$$U^n = U^{n-1}\ + \frac{\Delta t}{M}\ (W_X^n + W_X^a(t_n)) \tag{30}$$
$$Y^n = Y^{n-1} + \Delta t\, V^{n-1} + \frac{\Delta t^2}{2\ M}\ (W_Y^n + W_Y^a(t_n)) \tag{31}$$
$$V^n = V^{n-1}\ + \frac{\Delta t}{M}\ (W_Y^n + W_Y^a(t_n)) \tag{32}$$

where U^n (resp. V^n) approximates $X'(t_n)$ (resp. $Y'(t_n)$). This system is strongly nonlinear, since W_X^n and W_Y^n depend on X^n and Y^n. The proposed iterative strategy updates the dynamical variables X and Y simultaneously with the pressure and fluid fraction fields, as detailed in Table 2

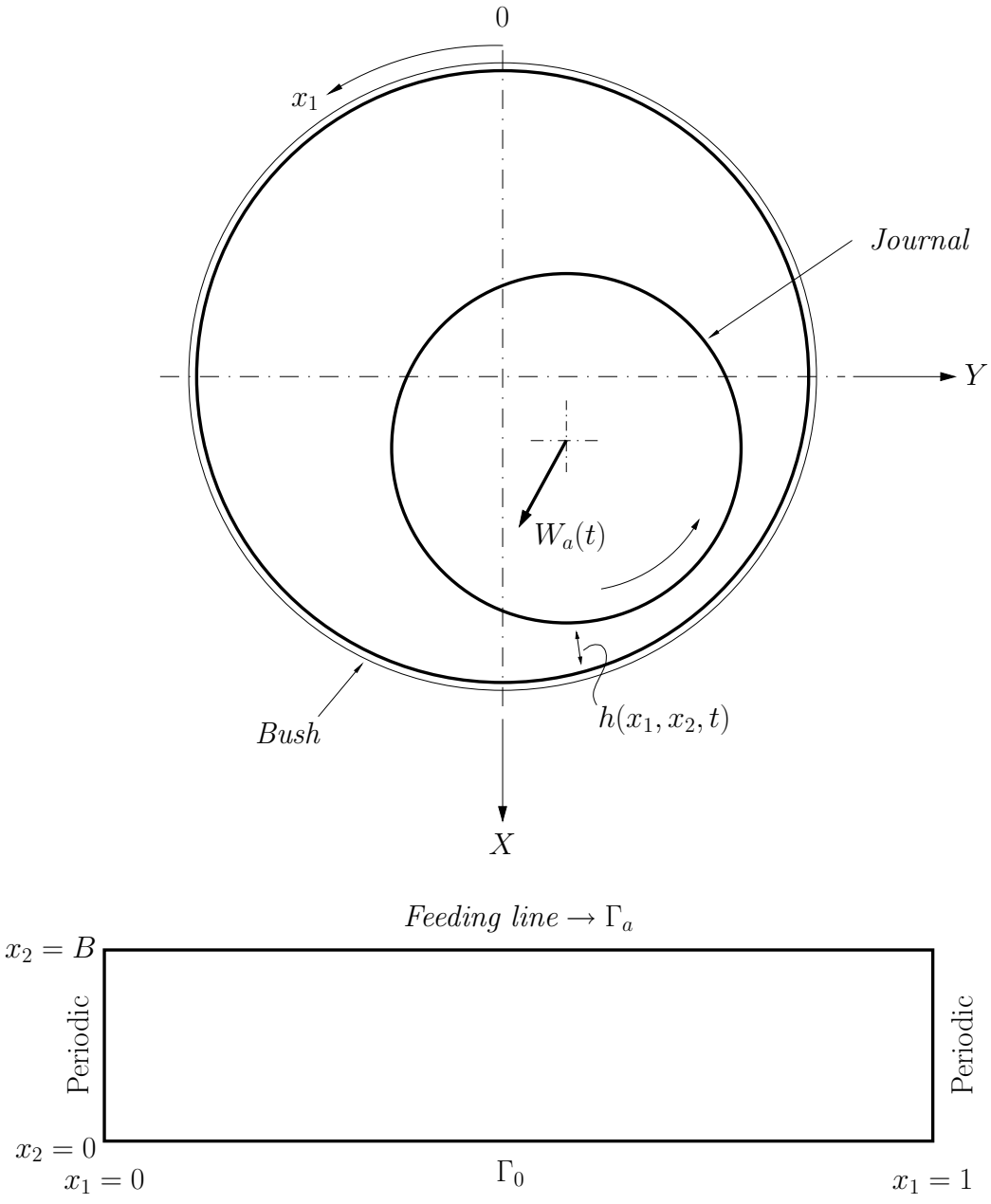

Figure 3: Schematic representation of the journal bearing and the computational domain considered.

Table 2: Iterative algorithm for dynamics.

do $(n = 1, \ldots, NT)$ *(Loop over time steps)*
  $t_n \;=\; n\,\Delta t, \quad k \;=\; 0$
  do $(i = 1, \ldots, N_1,\ j = 1, \ldots, N_2)$
    $p_{ij}^{n,0} \;=\; p_{ij}^{n-1}, \quad \theta_{ij}^{n,0} \;=\; \theta_{ij}^{n-1}$
  end do
  do while (*change* $>$ *tolerance*) *(Relaxation)*
    $k \;\leftarrow\; k + 1$
    $W_X^{n,k-1} = \Delta x_1\,\Delta x_2\ \sum_{i,j=1}^{N_1,N_2} p_{ij}^{n,k-1}\ \cos(2\pi\, i\,\Delta x_1)$
    $W_Y^{n,k-1} = \Delta x_1\,\Delta x_2\ \sum_{i,j=1}^{N_1,N_2} p_{ij}^{n,k-1}\ \sin(2\pi\, i\,\Delta x_1)$
    $X^{n,k} = X^{n-1} + \Delta t\, U^{n-1} + \frac{\Delta t^2}{2M}(W_X^{n,k-1} + W_X^a(t_n))$
    $Y^{n,k} = Y^{n-1} + \Delta t\, V^{n-1} + \frac{\Delta t^2}{2M}(W_Y^{n,k-1} + W_Y^a(t_n))$
    do $(i = 1, \ldots, N_1,\ j = 1, \ldots, N_2)$
      $h_{ij}^{n,k} \;=\; 1 + X^{n,k}\cos(2\pi i\Delta x_1) + Y^{n,k}\sin(2\pi i\Delta x_1)$
    end do
    do $(i = 1, \ldots, N_1,\ j = 1, \ldots, N_2)$
      if $(p_{i,j}^{n,k-1} > 0$ *or* $\theta_{i,j}^{n,k-1} == 1)$ ***then***
        Compute $P_{i,j}^{n,k}$ *using Eq. (17) with* $h^n = h^{n,k}$
        $p_{i,j}^{n,k} \;=\; \omega_p\ P_{i,j}^{n,k} + (1 - \omega_p)\ p_{i,j}^{n,k-1}$
        if $(p_{i,j}^{n,k} \geq 0)$ *(cavitation check)*
          $\theta_{i,j}^{n,k} = 1$
        else
          $p_{i,j}^{n,k} = 0$
        end if
      end if
      if $(p_{i,j}^{n,k} \leq 0$ *or* $\theta_{i,j}^{n,k} < 1)$ ***then***
        Compute $\Theta_{i,j}^{n,k}$ *using Eq. (18) with* $h^n = h^{n,k}$
        $\theta_{i,j}^{n,k} \leftarrow \omega_\theta\ \Theta_{i,j}^{n,k} + (1 - \omega_\theta)\ \theta_{i,j}^{n,k-1}$
        if $(\theta_{i,j}^{n,k} < 1)$ *(cavitation check)*
          $p_{i,j}^{n,k} = 0$
        else
          $\theta_{i,j}^{n,k} = 1$
        end if
      end if
    end do
    change $\;=\; ||\mathbf{p}^{n,k} - \mathbf{p}^{n,k-1}||_2 + ||\theta^{n,k} - \theta^{n,k-1}||_2 + |X^{n,k} - X^{n,k-1}| + |Y^{n,k} - Y^{n,k-1}|$
  end do
  $X^n \;=\; X^{n,k}, \quad Y^n \;=\; Y^{n,k}$
  $U^n \;=\; U^{n-1} \;+ \frac{\Delta t}{M}\ (W_X^{n,k-1} + W_X^a(t_n))$
  $V^n \;=\; V^{n-1} \;+ \frac{\Delta t}{M}\ (W_Y^{n,k-1} + W_Y^a(t_n))$
  do $(i = 1, \ldots, N_1,\ j = 1, \ldots, N_2)$
    $p_{ij}^n \;=\; p_{ij}^{n,k}, \quad \theta_{ij}^n \;=\; \theta_{ij}^{n,k}, \quad h_{ij}^n \;=\; h_{ij}^{n,k}$
  end do
end do *(End Loop over time steps)*

5 Second example: Journal bearing under dynamic loading

An essential test for a dynamical cavitation algorithm is that of transient loads typical of car engines, which essentially consist of two sharp impulses with a time interval of a quarter of a period. For this example, the non–dimensional period of the load is set to $T = 1$ and an analytical load given by (for $0 \leq t \leq 1$)

$$W_X^a(t) = 0.01 \left[\exp(-400(t-0.25)^2) + 0.95534 \exp(-400(t-0.5)^2)\right] \quad (33)$$

$$W_Y^a(t) = 0.29552 \times 10^{-2} \exp(-400(t-0.5)^2) \quad (34)$$

is choosen. The feeding pressure is set to $p_a = 0.0075$, the bearing width to $B = 0.1$, the journal mass to $M = 10^{-6}$ and the initial conditions to

$$\theta(x_1, x_2, t = 0) = 1, \quad X(t = 0) = Y(t = 0) = 0.5, \quad U(t = 0) = V(t = 0) = 0$$

The numerical parameters are chosen as

$$\Delta x_1 = \Delta x_2 = 5 \times 10^{-3}, \quad \Delta t = 10^{-3}, \quad \omega_p = \omega_\theta = 1, \quad \text{tolerance} = 10^{-6}$$

Under these conditions, the obtained evolution of the journal's center with time is as shown in Fig. 4, where the components of the applied load W_X^a, W_Y^a and those of the load capacity W_X and W_Y (changing its sign to ease the comparison with W_X^a and W_Y^a) are plotted as well. In Fig. 5 a detail of these loads is also shown. It can be seen that after one revolution of the shaft the system becomes periodic. The first impulse of the cycle suddenly brings the shaft, which was evolving freely (since no load is applied in the second half of the cycle), to the bottom center of the bush (near $X = 1$ and $Y = 0$). The inertia of the shaft creates a spike in the load (W_X and W_Y) at times 1.21, 2.21, etc. The second impulse takes it to another position (near $X = 0.86$ and $Y = 0.5$) and then the applied load becomes zero again until the first impulse of the next cycle.

A convergence study for this problem has been performed, running it on meshes of 100×10, 200×20, 400×40 and 800×80 cells. Two variables have been selected to illustrate this study: the maximum pressure $p_{\max}(t)$ and the eccentricity $e(t) = [X(t)^2 + Y(t)^2]^{1/2}$. In Fig. 6 $p_{\max}(t)$ is plotted between $t = 2$ and $t = 3$. Good agreement is found among all meshes, so that details of four subintervals are included ($2.10 \leq t \leq 2.15$, $2.21 \leq t \leq 2.22$, $2.25 \leq t \leq 2.27$ and $2.48 \leq t \leq 2.52$) in which the differences are visible. The error seems to behave linearly with the cell size (roughly speaking, the error reduces by half each time the cell size is halved), implying that the scheme is first-order accurate, which is a consequence of the upwind scheme used. It is also interesting to look at a plot of $e(t)$ between $t = 2$ and $t = 3$, which is shown in Fig. 7. The eccentricity attains its maximum value of 0.94 at $t = 2.56$ and then it remains practically constant until the next cycle. Notice however that this is not reproduced when the mesh is coarse (e.g., 100×10, in which case at $t = 3$ the eccentricity has fallen below 0.91). In this variable, again, the first-order-accurate behavior of the method is quite evident. For a resolution of 200×20 grid points, the computational cost of the algorithm was 12 minutes on a Pentium IV (3.0 GHz) processor to complete the three periods of time shown in the figures.

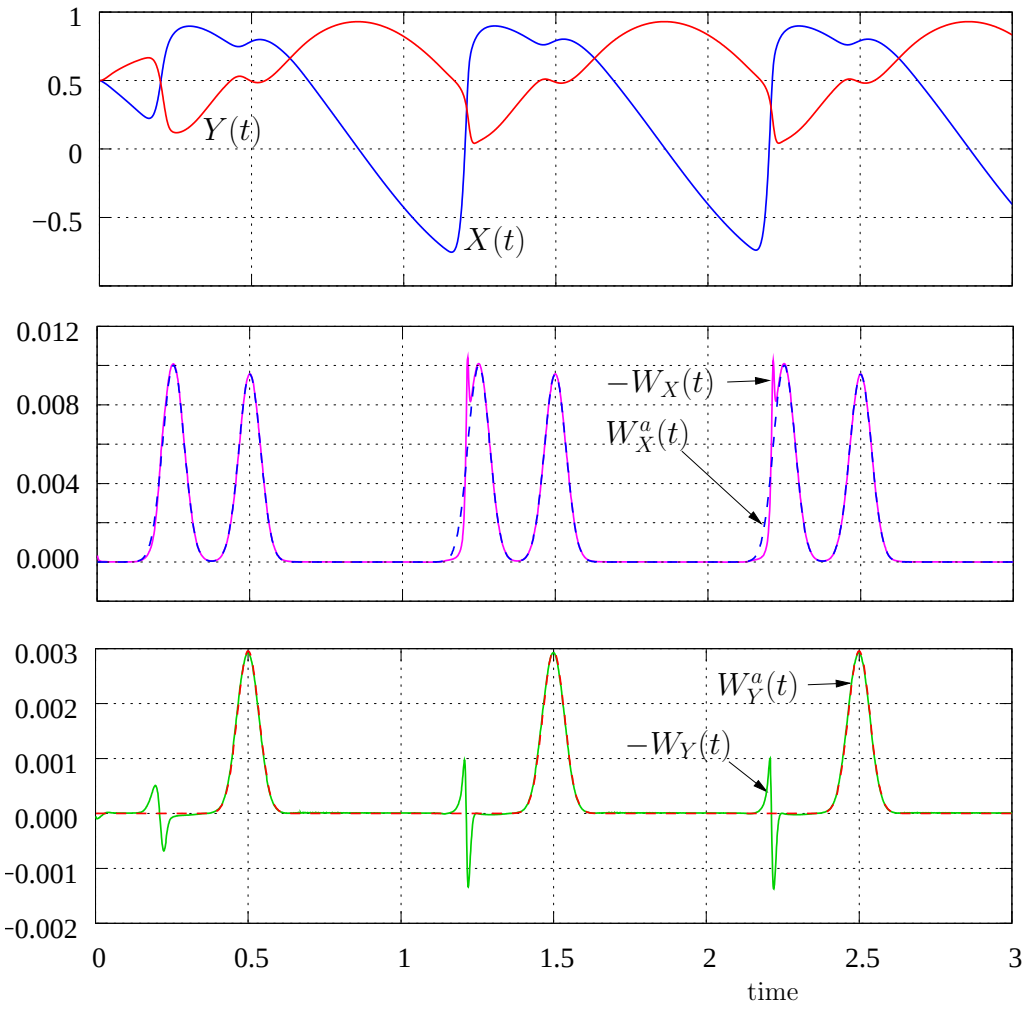

Figure 4: Evolution with time of the journal's center, applied loads W_X^a, W_Y^a and load capacity W_X and W_Y (changing its sign to ease the comparison W_X^a and W_Y^a).

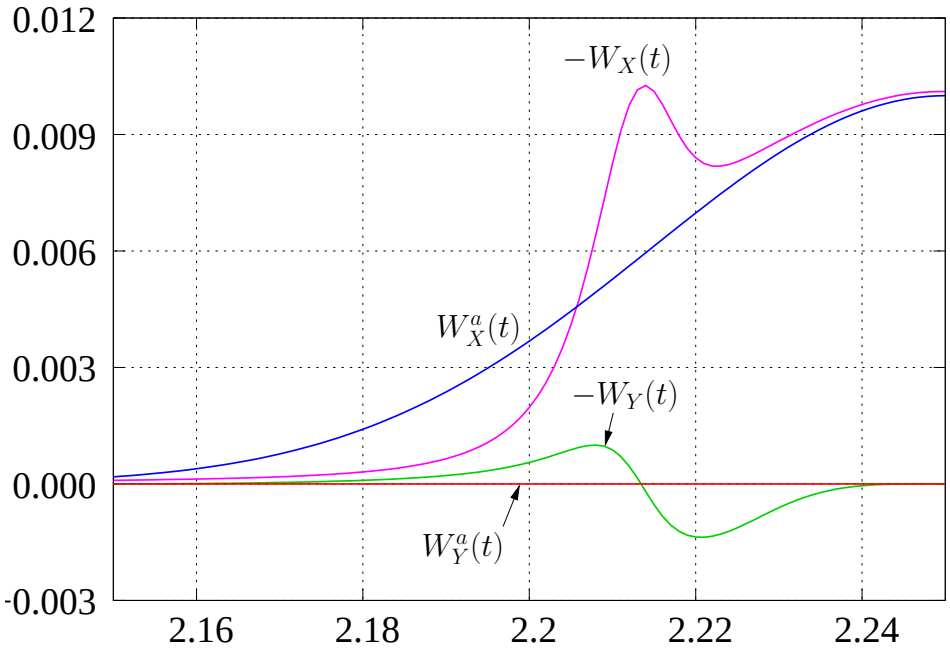

Figure 5: Detail of the evolution with time of the applied loads W_X^a, W_Y^a and load capacity W_X and W_Y (changing its sign to ease the comparison W_X^a and W_Y^a).

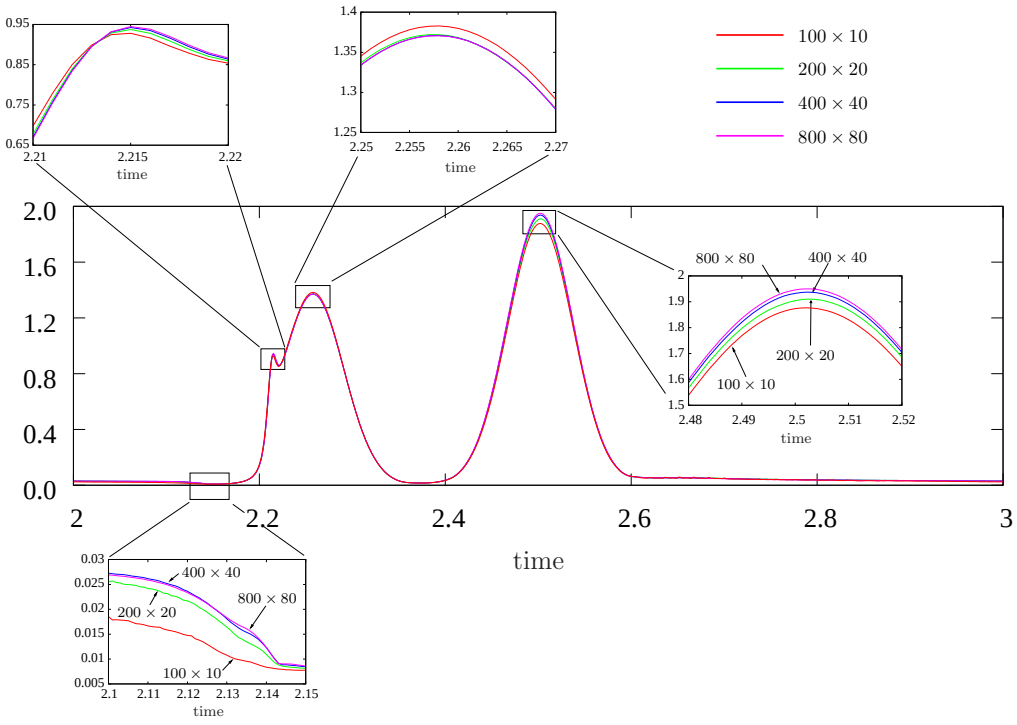

Figure 6: Convergence study: evolution with time of the maximum value of the pressure.

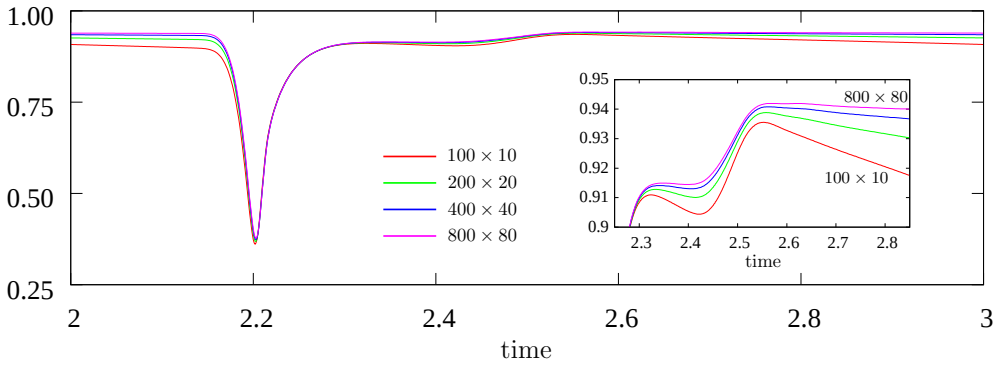

Figure 7: Convergence study: evolution with time of the eccentricity.

6 Summary

The aim of this article has been to introduce a simple, robust and freely available methodology to numerically solve dynamical lubrication problems modeled with a mass-conserving formulation. This was done first in the case in which the gap-thickness is a known function of time, and then in the fully-dynamical case. Each case was illustrated with a detailed example, and the reader is invited to download the code and get the full set of numerical results. In many fields of science the availability of open source codes has proved useful in vaious ways: making it easier for students to start their research, setting standards with which to compare new techniques, and enabling engineers that do not specialize in numerics to carry out simulations without buying expensive commercial codes, among others. This article is aimed at making a contribution in this direction.

ACKNOWLEDGMENTS: Partial support provided by CNEA (Argentina), ANPCyT (Argentina) CNPq (Brazil) and FAPESP (Brazil) is gratefully acknowledged. RFA receives an schollarship from CONICET (Argentina).

References

[1] Elrod, H. G. and Adams, M., 1974, "A computer program for cavitation and starvation problems. Technical report 190." 1st LEEDS LYON Symposium on Cavitation and Related Phenomena in Lubrication, I.M.E., **103**, pp. 37–41.

[2] Geike, T. and Popov, V., 2009, "Cavitation within the framework of reduced description of mixed lubrication," Tribology International, **42**, pp. 93–98.

[3] Jakobsson, B. and Floberg, L., 1957, "The finite journal bearing considering vaporization," Tran. Chalmers University of Tech. Gothenburg.

[4] Olsson, K., 1965, "Cavitation in dynamically loaded bearings," Tran. Chalmers University of Tech. Gothenburg.

[5] Ausas, R., Ragot, P., Leiva, J., Jai, M., Bayada, G., and Buscaglia, G., 2007, "The impact of the cavitation model in the analysis of micro-textured lubricated journal bearings," ASME Journal of Tribology, **129**, pp. 868–875.

[6] Kumar, A. and Booker, J., 1991, "A finite element cavitation algorithm," ASME Journal of Tribology, **113**, pp. 261–276.

[7] Vijayaraghavan, D. and Keith, T., 1989, "Development and evaluation of a cavitation algorithm," STLE Trib. Trans., **32**, pp. 225–233.

[8] Bonneau, D., Guines, J., Frêne, J., and Toplosky, J., 1995, "Ehd analysis, including structural inertia effects and mass–conserving cavitation model," ASME Journal of Tribology, **117**, pp. 540–547.

[9] Optasanu, V. and Bonneau, D., 2000, "Finite element mass-conserving cavitation algorithm in pure squeeze motion. validation/application to a connecting rod small end bearing," Transactions of the ASME, **122**, pp. 162–169.

[10] Hajjam, M. and Bonneau, D., 2007, "A transient finite element algorithm with application to radial lip seals," Tribology International, **40**, pp. 1258–1269.

[11] Bayada, G. and Chambat, M., 1984, "Existence and uniqueness for a lubrication problem with non regular conditions on the free boundary," Boll. U.M.I., **6,3b**, pp. 543–557.

[12] Bayada, G. and Chambat, M., 1986, "Sur quelque modelisation de la zone de cavitation en lubrification hydrodynamique." Journal de Mécanique Théorique et Appliquée, **5**, pp. 703–729.

[13] Boedo, S. and Booker, J., 1995, "Cavitation in normal separation of square and circular plates," ASME Journal of Tribology, **117**, pp. 403–409.